Geometry-driven out-of-plane magnetization states in nanostructures

A. Maziewski,[1] V. Zablotskii,[1,2] and M. Kisielewski[1]
[1]*Institute of Experimental Physics, University of Bialystok, Lipowa 41, 15-424 Bialystok, Poland*
[2]*Institute of Physics ASCR, Na Slovance 2, 18221 Prague 8, Czech Republic*
(Received 17 February 2006; published 14 April 2006)

Magnetization states of laterally limited ultrathin nanostructures (semi-infinite film edges, wires, and disks) with low magnetic uniaxial anisotropy are studied analytically and by micromagnetic simulations. A general view of geometrically constrained magnetization distributions is given. By shrinking the lateral size of a sample one can induce reorientation from an in-plane to an out-of-plane magnetization state. As examples, magnetic phase diagrams have been calculated for cobalt nanowires and disks. In low-anisotropy nanodisks magnetization distributions like an out-of-plane domain-patterned vortex and a domain-patterned leaf are found.

DOI: 10.1103/PhysRevB.73.134415 PACS number(s): 75.70.Ak, 75.40.Mg, 75.60.Ch, 75.70.Kw

Magnetism on the nanometer scale is a subject of great interest in view of both the development of fundamental knowledge and its possible applications. Out-of-plane magnetization states are now especially topical because of the new generation of high-density devices. Out-of-plane magnetization states are more robust against thermal flips of nanosized domains than is in-plane spin geometry.[1] Modern technologies (such as electron beam lithography and the focused ion beam technique or x-ray interference lithography in combination with electrodeposition) give the opportunity to produce nanostructures with high-precision geometry as well as magnetic properties. High-spatial-resolution techniques enable experimental analysis of magnetization distributions on the nanoscale length, e.g., see Refs. 1–4.

The geometry of nanomagnets may stabilize different magnetic states, e.g., geometrically and anisotropy constrained walls, vortices, buckles, leaves, and flowers.[5–8] The geometry change induces transitions between these magnetization configurations and strongly affects the magnetization processes.[7] For many low-thickness nanostructures perpendicular magnetic anisotropy is expected,[9] which is usually characterized by the Q_1 $(=K_1/2\pi M_S^2)$ parameter, where K_1 and M_s are the first uniaxial anisotropy constant and the saturation magnetization, respectively. Thickness-driven changes of Q_1 can induce the reorientation phase transition (RPT) from the perpendicular to the in-plane magnetization state. In laterally infinite films the RPT occurs at the thickness d_1 defined by $Q_1(d_1)=1$ for a monodomain state. Magnetization distributions with nanosized domains were experimentally studied[10] in ultrathin cobalt wedges near the RPT. It has been recently shown that in ultrathin films magnetization reorientation between the perpendicular and in-plane states is accompanied by the appearance of sinusoidal-like domains whose magnetostatic contribution increases the Q range of the out-of-plane magnetization state. Approaching the RPT the domain period decreases down to the minimal value $p^* \approx 8\pi l_{ex}^2/d$ (where $l_{ex}=[A/(2\pi M_S^2)]^{1/2}$ is the exchange length, A is the exchange constant, and d is the film thickness).[11] In comparison with infinite films, the range of the out-of-plane magnetization state can be significantly extended by shrinking the sample lateral sizes.[12] Such an extension was also shown by Monte Carlo simulations performed for nanoplatelets with $Q_1=0.9$.[13] The role of the finite-size effect on phase transitions in ferroelectric nanodisks and nanorods was recently demonstrated in Ref. 14.

A general view of the out-of-plane magnetization state extension is the purpose of our work. We study magnetization distributions in the three following geometries: semi-infinite film edges, wires, and disks; all with different Q_1. The proposed analytical description is supported by micromagnetic simulations using OOMMF software.[15] Results are illustrated for ultrathin cobalt with typical thickness dependence of $Q_1(d)=(K_{1v}+2^*K_{1S}/d)/2\pi M_S^2$ (with $K_{1v}=1.9\times10^7$ erg/cm^3 and $K_{1s}=0.57$ erg/cm^2) and $l_{ex}=3.2$ nm.[6]

The Q-driven evolution of magnetization distributions at the edge of a semi-infinite film was recently studied by simulations in Ref. 12. It was shown that the RPT induced by decreasing Q is accompanied by a sinusoidal domain structure with the decaying amplitude and period which is close to p^* predicted for domains in laterally infinite films.[11] In the case of a thickness-driven RPT, as the film thickness increases the edge amplitude $[m_z(x=0)]$ falls to zero at $d=d_{edge}$. The thickness dependence of the $m_z(x=0)$ amplitude is well described by the function $m_z(d)=C(d_{edge}-d)^b$, where $d_{edge}=2.27$ nm and $b=0.5$.[12] This is a typical scaling law, describing the critical behaviors. Due to the demagnetizing field cutoff, the edge induces a significant increase of the range of out-of-plane magnetization states. Indeed, as shown in Ref. 12 nonzero m_z exists near the film edge down to $Q_{1edge}\approx0.89$ or for $d\leqslant d_{edge}$ which is much higher than d_1 defining the RPT in infinite films.

In order to find the critical thickness d_{edge} when magnetization becomes pure-in plane let us consider the balance of torques acting at the edge spins (a similar method was used in Refs. 16 and 17). In equilibrium the sum of torques produced by the demagnetizing, anisotropy, and exchange fields is zero:

$$\Gamma_{dem}+\Gamma_{an}+\Gamma_{ex}=0 \tag{1}$$

where $\Gamma=-dE/d\theta$, E represents the corresponding energies, and θ is the angle between the magnetization vector and film

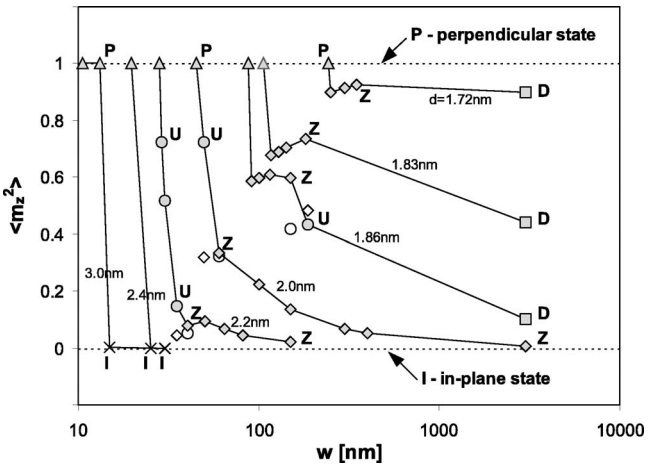

FIG. 1. Map of magnetization states: $\langle m_z^2 \rangle$ as a function of the wire width for different thicknesses. Filled and open symbols mark $\langle m_z^2 \rangle$ for equilibrium and metastable states, respectively.

normal. Using the energy densities $E_{dem}=-(H_{dem}M_S)/2$, $E_{an}=K\sin^2\theta(x)$, and $E_{ex}=Ad^2\theta(x)/dx^2$, by virtue of spatial averaging of Eq. (1) over distance L, one can arrive at

$$[Q_1(d)-\langle h_{dem}\rangle]\sin 2\varphi(0)=l_{ex}^2\frac{d^2\varphi(0)}{dx^2} \tag{2}$$

where $\varphi(0)$ denotes the angle between the magnetization vector and the film plane, and $\langle h_{dem}\rangle=\langle H_{dem}\rangle/4\pi M_S$. On the right side of Eq. (2) the second derivative can be replaced by $\varphi''(0)=\varphi(0)/L^2$, where L is a characteristic length on which the magnetization orientation essentially changes. The demagnetization field of a slab of width L and thickness d can be analytically calculated using formulas given in Ref. 4. Below we use $L=p^*/4$ because $\varphi(p/4)=0$, whose value is close to the coherent rotation length $R=p/2=22.78l_{ex}^2/2d$.[18] The RPT takes place when the edge amplitude $\varphi(0)\to 0$. Thus, applying the limit to Eq. (2), one can obtain

$$Q_1(d)=\langle h_{dem}(d/p^*)\rangle+\frac{d^2}{8\pi l_{ex}^2}. \tag{3}$$

In the limiting case when $d\to 0$, $\langle h_{dem}\rangle=\langle h_{dem}(0)\rangle=1$, and Eq. (3) turns into the RPT condition for infinite films: $Q_1(d)=1$. Equation (3) allows us to calculate the RPT critical thickness d_{edge} for semi-infinite ultrathin films. For example, for ultrathin Co/Au the numerical solution of Eq. (3) gives $d_{edge}=2.17$ nm.

Let us consider results of simulations of magnetization distributions in right-prism-shaped nanowires with width w. Figure 1 shows the evolution of magnetization distribution with changes of both d and w. The three critical thicknesses d_1, d^*, and d_{edge} determine four scenarios of the phase transition to the perpendicular homogeneous state which take place as the wire width is gradually squeezed. We denote the magnetization phases as follows: I, the homogeneous in-plane state; P, the homogeneous perpendicular state; D, a multidomain state consisting of domains with perpendicular magnetization components; U, a magnetization distribution having mirror symmetry [U-shaped profile of $m_z(x)$; see Figs. 2(b) and 2(c)]; and Z, a magnetization distribution having an inverted center [Z-shaped profile of $m_z(x)$; Figs. 2(a)–2(c)]. These magnetization states we characterize by $\langle m_z^2 \rangle$ averaged over the whole sample; it defines a convenient measure of "magnetization perpendicularity." A wire squeezing (starting from width $w=3000$ nm) influence on magnetization distribution is shown in Fig. 2.The following phase transitions channels, obtained by simulations, are shown in Fig. 2.

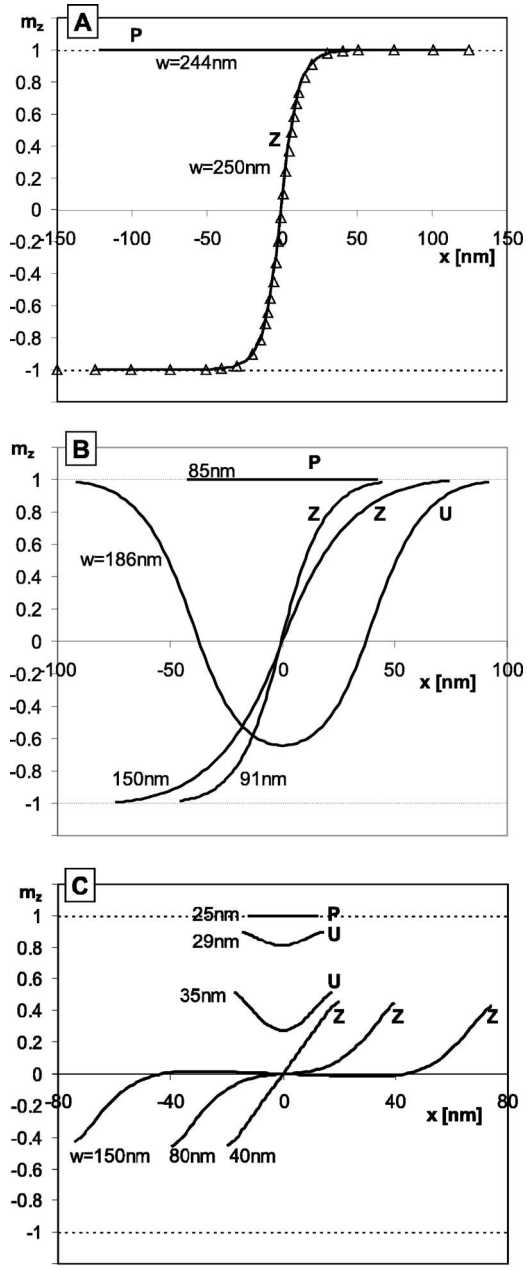

FIG. 2. Magnetization profiles $[m_z(x)]$ for different wire widths and thicknesses. (a) $d=1.72$ ($<d_1$) and $w=244$ and 250 nm. Triangles marks $m_z(x)$ calculated for infinite film. (b) $d=1.86$ (slightly below d^*) and $w=85-186$ nm. (c) $d^*<d=2.2$ nm$<d_{\text{edge}}$ and $w=25-150$ nm.

The first transition channel is open for wires with $d<d_1$. As w decreases the number of domains ($N=18$ for w

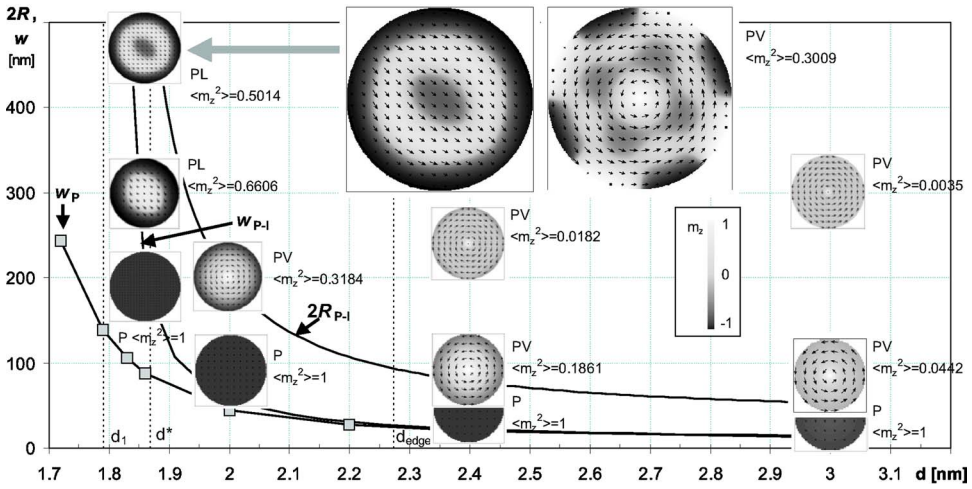

FIG. 3. (Color online) Magnetic configurations of wires and disks. From bottom to top: $w_P(d)$ is the upper wire width of the existence of the pure P state; $w_{P\text{-}I}(d)$ and $2R_{P\text{-}I}(d)$ are the phase equilibrium curves of homogeneous P and I states in wire and disk, respectively. Inset shows the magnetization states of the disk with $d=1.86$ nm and $2R=476$ nm: the out-of-plane domain patterned leaf (PL) and vortex (PV).

$=3000$ nm) decreases on approaching $N=2$ for $w=250$ nm [see Fig. 2(a)]. The magnetization distribution in the wall separating these domains is similar to the distribution in the Bloch-like wall in an infinite film described by triangles in Fig. 2(a). Further w shrinking leads to a jump into the monodomain perpendicular state ($Z\rightarrow P$); see the distribution for $w=244$ nm. The second channel is open for wires with $d_1<d<d^*$. As w decreases, the number of domains decreases, while the average amplitude of magnetization increases. There is the phase sequence $D\rightarrow U\rightarrow Z\rightarrow P$. Figure 2(b) shows the w-decrease-induced evolution $U\rightarrow Z\rightarrow P$ determined for thickness slightly below d^*, where there is a strong influence of demagnetization forces in the volume of the whole wire. Finally, the squeezing leads to a jump into the P state. In the third channel ($d^*<d<d_{edge}$) the phase sequence is $Z\rightarrow U\rightarrow P$. For a wide enough wire, domain states do not exist if $d>d^*$.[11] The edges affect out-of-plane magnetization distortion only near the ends of a wide wire.[12] On shrinking the lateral size, the area of almost in-plane magnetization decreases while the areas of out-of-plane magnetization do not significantly change. The area with $m_z\approx 0$ has a small contribution to the total system energy so it is easily squeezed. The jump $Z\rightarrow U$ occurs when the area with $m_z\approx 0$ vanishes; see $m_z(x)$ for wires with widths 40 and 35 nm in Fig. 2(c). The U-shaped distribution evolves into the P state, further decreasing w. In the fourth channel ($d>d_{edge}$) a jumplike transition $I\rightarrow P$ takes place. The squeezing-induced evolution of magnetization distributions into the perpendicular state may occur through either equilibrium states or metastable ones. Some metastable states are marked in Fig. 1 by open symbols. Thus, magnetichistory could influence the evolution in a real sample.

To describe the RPT in rectangular-shaped nanowires let us consider the energy balance between perpendicular and in-plane magnetization states $E_\perp=E_\parallel$. The balance gives

$$Q_1(d)+Q_2(d)=\langle h_{dem}\rangle=\frac{1}{wd}\int_0^d\int_0^w h_{dem}(x,z)dz\,dx, \quad (4)$$

where the space-averaged $\langle h_{dem}\rangle$ is a function of the d/w ratio, $Q_2=K_2/2\pi M_S^2$, and K_2 is the second-order anisotropy constant. In the case of an "infinite" film d/w becomes 0 and $\langle h_{dem}\rangle=1$ which corresponds to $Q_1=1$—i.e., the RPT condition for infinite films (neglecting higher orders of anisotropy constants). Defining the P-I phase equilibrium curve, Eq. (4) connects the material (Q) and the geometrical parameters of the sample. Using the linear approximation $\langle h_{dem}\rangle\approx 1-cd/w$ dependence where $c=1.2$, in the range of interest $0\leqslant d/w\leqslant 0.25$, the approximation gives an error less than 5%) and $Q_1(d)$, one can analytically obtain the critical wire width $w_{P\text{-}I}$ as a function of the thickness. So, from Eq. (4) one can arrive at the approximation

$$w_{P\text{-}I}\approx\frac{cd_1d^2}{d_0(d-d_1)} \quad (5)$$

where $d>d_1$ and $d_0=K_{1S}/\pi M_S^2$ (=0.9 nm for the given above constants). The numerical solution of Eq. (4)—the curve of the phase equilibrium between the in-plane and perpendicular homogeneous states—$w_{P\text{-}I}(d)$ is plotted in Fig. 3. The $w_P(d)$ obtained by simulations—the upper width limit of existence of the pure perpendicular state—is also plotted in Fig. 3. Both $w_{P\text{-}I}(d)$ and $w_P(d)$ curves coincide for $d>d_{edge}$. This implies that the jumplike transition $P\rightarrow I$ must take place here, as illustrated in Fig. 1 for $d=3$ and 2.4 nm. At $d=d_{edge}$ the $w_{P\text{-}I}(d)$ and $w_P(d)$ curves split, opening a zone with the sequences of nonuniform magnetization distributions for $d<d_{edge}$ discussed above. The curve crossover defines the three-critical point.

Now we consider magnetization distributions in disks of radius R. The symmetry favors a more pronounced edge effect disturbing the in-plane magnetization configuration and extending the range of the out-of-plane magnetization configuration. The geometry induces a vortex-type magnetization distribution in low-anisotropy cases. Simulations show that out-of-plane magnetization states exist even for disks for small Q (e.g., $d>d_{edge}$); see the vortexlike magnetization distribution in Fig. 3 ($R=300$ nm and $d=3$ nm). Squeezing the disk diameter leads to a patterned vortex state (PV) and finally to the transition into the purely perpendicular state (P). Decreasing R, a similar magnetization distribution evolution PV$\rightarrow P$ occurs; see the distributions for $d=2.4$ and 2 nm in Fig. 3. Notice that by decreasing d the out-of-plane amplitude increases. When $d<d^*$ and the disk radius is large

enough, the PV state has higher energy than that of the patterned leaf (PL); see Fig. 3 (inset). Figure 3 shows the transition PL$\rightarrow P$ induced by decreasing R for $d=1.86(<d^*)$.

In order to estimate the critical thickness, once again we analyze the energy balance between the perpendicular and in-plane magnetization states. For a pure perpendicular magnetization state, the total energy is provided by the magnetostatic contribution while for the in-plane state the total energy is provided by both anisotropy and magnetostatic energy caused by the magnetic poles on the side cylinder surface. By means of the demagnetization factors one can take into account the contribution of the poles. So, in terms of the demagnetization factor, the energy balance ($E_\perp = E_\parallel$) can be written as

$$Q_1(d) = f\left(\frac{2R}{d}\right) = N_{ax}\left(\frac{2R}{d}\right) - N_{di}\left(\frac{2R}{d}\right) \tag{6}$$

with rigorous[19] expressions for the axial demagnetization

$$N_{ax}(k) = 1 + \frac{4k}{3\pi} - \frac{{}_2F_1[5/2, 1/2; 2; k^2/(1+k^2)]}{\sqrt{1+k^2}}$$

and the diametric demagnetization $N_{di}(k)=[1-N_{ax}(k)]/2$ factors, where ${}_2F_1$ is the hypergeometric Gauss function. $k=2R/d$ is the aspect ratio. The numerical solution of Eq. (6) is plotted in Fig. 3 as $2R_{P\text{-}I}(d)$. As seen from this figure the critical thickness grows, shrinking the lateral sample size. In the limiting case $R\rightarrow\infty$ $f(2R/d)$ goes to 1, and therefore Eq. (6) gives $Q_1(d)=1$ or $d=d_1$. Note that for the smallest aspect ratio the influence of the discrete dipole lattice on the obtained results can be taken into account by inserting into Eq. (6) the lattice-dependent "x prefactor" introduced in Ref. 19. The next possible generalization of our approach is related to the enhanced anisotropy contribution of the edge atoms. It was recently reported in Ref. 20 that in cobalt nanometer-sized particles the edge atoms have 20 times more anisotropy energy than their bulk and surface counterparts. In Eqs. (4) and (6) this anisotropy contribution could be taken into account by adding a term describing a Q_1 contribution of atoms sitting at the outer perimeter of the sample. The $2R_{P\text{-}I}(d)$ curve represents the phase equilibrium line separating the homogeneous perpendicular and in-plane phases. The pure perpendicular state in disks, as in wires, exists for smaller lateral size, $R<R_{P\text{-}I}$. Lines separating vortex and single-domain magnetization states of disks were recently found by theory[7,8,21] and experiment[22] for nanodisks with negligible small Q_1. In Ref. 23 concentric domains were found by simulations in Ni disks with $Q_1=0.94$.

In conclusion, in nanomagnets with low perpendicular anisotropy, out-of-plane magnetization states can be achieved by varying the sample geometry and/or lateral size for any convenient thickness. This opens the way to stabilizing and driving confined magnetic configurations; for example, the spin reorientation transition can be manipulated by matching the magnetic and geometrical parameters of nanoelements. The edge cutoff of the demagnetizing field has been found to be responsible for extended out-of-plane magnetization states in wires. In nanowires four scenarios of the transition to the out-of-plane magnetization state can be distinguished (see Fig. 1). In disks the out-of-plane states are caused by both the edge cutoff and edge curling effects. In terms of a unified approach for disks and wires we have obtained the relationships between the geometrical and material parameters [Eqs. (4)–(6)] allowing calculations of phase equilibrium curves separating the perpendicular and in-plane magnetization states. The following nanoscaled magnetization distributions have been found: Z- and U-shaped magnetization profiles in wires; out-of-plane domain-patterned vortices and leaves corresponding to the ground or metastable magnetization states of nanodisks. The obtained results reveal the precise role of the finite-size effect on the existence of multistable magnetization states and phase transitions in low-dimensional structures. The geometry-driven magnetization distributions found seem to open new areas for experimental studies (especially using high-precision patterning and high-resolution magnetization distribution analysis techniques) and possible applications, e.g., related to perpendicular recording.

This work was supported by the Polish State Committee for Scientific Research (Grant No. 4 T11B 006 24) and the Marie Curie Foundation ("NANOMAG-LAB" Grant No. N 2004-003177).

[1] M. Bode, O. Pietzsch, A. Kubetzka, and R. Wiesendanger, Phys. Rev. Lett. **92**, 067201 (2004).
[2] A. Wachowiak, J. Wiebe, M. Bode, O. Pietzsch, M. Morgenstern, and R. Wiesendanger, Science **298**, 577 (2002).
[3] K. von Bergmann, M. Bode, A. Kubetzka, O. Pietzsch, and R. Wiesendanger, Microsc. Res. Tech. **66**, 61 (2005).
[4] A. Hubert and R. Schäfer, *Magnetic Domains* (Springer, Berlin 1998).
[5] P. Bruno, Phys. Rev. Lett. **83**, 2425 (1999).
[6] M. Kisielewski, A. Maziewski, M. Tekielak, A. Wawro, and L. T. Baczewski, Phys. Rev. Lett. **89**, 087203 (2002).
[7] R. P. Cowburn, J. Phys. D **33**, R1 (2000).
[8] R. P. Cowburn and M. E. Welland, Appl. Phys. Lett. **72**, 2041 (1998).
[9] *Ultrathin Magnetic Structures*, edited by B. Heinrich and J. A. C. Bland (Springer, Berlin, 1994).
[10] M. Speckmann, H. P. Oepen, and H. Ibach, Phys. Rev. Lett. **75**, 2035 (1995).
[11] M. Kisielewski, A. Maziewski, T. Polyakova, and V. Zablotskii, Phys. Rev. B **69**, 184419 (2004).
[12] M. Kisielewski, A. Maziewski, and V. Zablotskii, J. Magn. Magn. Mater. **290-291**, 776 (2005).
[13] E. Y. Vedmedenko, H. P. Oepen, and J. Kirschner, Phys. Rev. B **67**, 012409 (2003).
[14] I. I. Naumov, L. Bellaiche, and Huaxiang Fu, Nature (London) **432**, 737 (2004).

[15] M. Donahue and D. Porter, http://math.nist.gov/oommf
[16] W. Rave, K. Ramstöck, and A. Hubert, J. Magn. Magn. Mater. **183**, 329 (1998).
[17] O. Fruchart, B. Kevorkian, and J. C. Toussaint, Phys. Rev. B **63**, 174418 (2001).
[18] R. Skomski, H. P. Oepen, and J. Kirschner, Phys. Rev. B **58**, 3223 (1998).
[19] Y. T. Millev, E. Vedmedenko, and H. P. Oepen, J. Phys. D **36**, 2945 (2003).
[20] S. Rusponi, T. Cren, N. Weiss, M. Epple, P. Buluschek, L. Claude, and H. Brune, Nat. Mater. **2**, 546 (2003).
[21] P.-O. Jubert and R. Allenspach, Phys. Rev. B **70**, 144402 (2004).
[22] A. Yamasaki, W. Wulfhekel, R. Hertel, S. Suga, and J. Kirschner, Phys. Rev. Lett. **91**, 127201 (2003).
[23] J. K. Ha, R. Hertel, and J. Kirschner, Europhys. Lett. **64**, 810 (2003).